J. Plasma Physics (2006), *vol.* 72, *part* 4, *pp.* 571–585.
doi:10.1017/S0022377805004277 First published online 11 January 2006 Printed in the United Kingdom

The coupling of shear and fast Alfvén waves at a magnetic X-point

K. G. McCLEMENTS[1], N. SHAH[2] and A. THYAGARAJA[1]

[1]EURATOM/UKAEA Fusion Association, Culham Science Centre, Abingdon, Oxfordshire OX14 3DB, UK

[2]University of Bath, Bath BA2 7AY, UK
(k.g.mcclements@ukaea.org.uk)

(Received 4 August 2005 and in revised form 10 August 2005; accepted 10 August 2005)

Abstract. The coupling of shear and fast Alfvén waves in the vicinity of a magnetic X-point is studied for the case in which a weak longitudinal guide field B_{z0} is present, with variations in the longitudinal direction and plasma pressure effects neglected. It is shown that an analytical solution for the shear wave in the limit of ideal magnetohydrodynamics (MHD) and $B_{z0} = 0$ exhibits phase mixing and equilibration of the field and kinetic energy at a rate that increases with the spatial extent of the initial disturbance. Equations describing perturbatively the pumping of fast waves by shear waves in the presence of finite B_{z0} are derived and solved numerically, taking into account resistivity and electron inertial effects. It is shown that shear wave energy is most rapidly and efficiently converted to plasma kinetic energy when the collisionless skin depth exceeds the resistive scale length. The conversion of incompressible MHD modes to compressible modes at X-points provides a possible mechanism for solar coronal heating, and mode conversion processes of this type are also likely to occur in tokamak plasmas with X-points.

1. Introduction

Magnetic X-points occur frequently in both natural and laboratory plasmas, and are of considerable theoretical interest, since they provide a simple paradigm for the study of a wide range of plasma phenomena, such as magnetohydrodynamic (MHD) mode conversion (Bulanov et al. 1992), magnetic reconnection (Craig and Watson 1992; McClements et al. 2004) and particle acceleration (Bulanov 1980; Bruhwiler and Zweibel 1992; Petkaki and MacKinnon 1997; Mori et al. 1998; Browning and Vekstein 2001; Hamilton et al. 2003, 2005). In the solar context, it has been proposed that X-points could play an important role in both coronal heating (Hassam and Lambert 1996) and flare energy release (Craig and McClymont 1991). In laboratory tokamak experiments, X-points in the poloidal component of the magnetic field can occur both inside the plasma due to magnetic reconnection (see, e.g., Donné et al. 2005) and, in the case of divertor operation, at the plasma edge. In the latter case it is very likely that there is a causal link between the presence of X-points and the achievement of enhanced ('H-mode') confinement, but a full physical understanding of the impact of X-points on tokamak plasma stability and confinement has yet to be achieved.

Previous authors have demonstrated that even the simplest type of current-free plasma X-point configuration, with no longitudinal guide field, has a rich physical

structure (see, e.g., Bulanov and Syrovatskii 1980). This is particularly so when non-MHD effects are take into account (McClements and Thyagaraja 2004). However, the presence of a longitudinal field B_{z0} cannot be neglected in the tokamak case, and Bulanov et al. (1992) have argued that taking B_{z0} to be exactly equal to zero is a rather restrictive assumption. Neglecting electrical resistivity and plasma pressure effects, these authors studied analytically the coupling of shear Alfvén waves and fast Alfvén waves at an X-point with zero equilibrium current but finite B_{z0}. When $B_{z0} = 0$ the two modes are decoupled, provided that there are no variations in the longitudinal direction (Bulanov and Syrovatskii 1980). The present paper is also concerned with the coupling of shear and fast Alfvén waves at an X-point with $B_{z0} \neq 0$. Our approach differs from that of Bulanov et al. (1992) in that we include resistive and non-MHD effects, and we impose boundary conditions that ensure zero Poynting flux out of the system. This enables us to focus on the issue of how rapidly the energy in a shear wave is dissipated or transformed into other forms of energy at an X-point with $B_{z0} \neq 0$.

Following the derivation in Sec. 2 of a particular shear Alfvén wave solution of the linearized ideal MHD equations for an X-point with $B_{z0} = 0$, we present in Sec. 3 a perturbative analysis of the coupling of shear waves and fast waves at an X-point with finite B_{z0}. Possible implications of our results for solar and laboratory plasmas are discussed in Sec. 4.

2. Shear wave at X-point with zero longitudinal field

As indicated previously, shear and fast waves propagating in the vicinity of a current-free X-point are decoupled if there are no variations in the longitudinal direction and zero magnetic field in that direction; moreover, in the ideal limit the equations describing both types of mode can be readily solved analytically (Bulanov and Syrovatskii 1980; Bulanov et al. 1992; McLaughlin and Hood 2004). Here we evaluate one particular solution for the shear wave, focusing on the temporal behaviour of the field energy and kinetic energy. This solution will be invoked in the next section as a drive for the fast wave in the presence of a weak longitudinal field.

We consider perturbations of the following equilibrium magnetic field configuration:

$$\mathbf{B}_{\mathrm{E}} = \frac{B_0}{r_0}(y\hat{\mathbf{x}} + x\hat{\mathbf{y}}), \tag{1}$$

where B_0 is the field at radial distance r_0 from the null, with $\hat{\mathbf{x}}$ and $\hat{\mathbf{y}}$ denoting unit vectors in the x and y directions. The system is assumed to be invariant in the z-direction. In the limit of zero plasma pressure and in the absence of equilibrium flows, the linearized ideal MHD induction and momentum equations can be written as

$$\frac{\partial \mathbf{B}}{\partial t} = \nabla \times (\mathbf{v} \times \mathbf{B}_{\mathrm{E}}), \tag{2}$$

$$\frac{\partial \mathbf{v}}{\partial t} = \frac{1}{\mu_0 \rho_0}(\nabla \times \mathbf{B}) \times \mathbf{B}_{\mathrm{E}}. \tag{3}$$

Here, $\mathbf{B}$ and $\mathbf{v}$ are the perturbations to the magnetic field and fluid velocity, ρ_0 is the equilibrium density (assumed to be uniform) and μ_0 is free space permeability.

https://doi.org/10.1017/S0022377805004277 Published online by Cambridge University Press

Normalizing the space coordinates x and y to r_0, time t to the Alfvén time $r_0(\mu_0\rho_0)^{1/2}/B_0$, B_z to B_0 and v_z to the Alfvén speed at $r = r_0$, we find that the z-components of (2) and (3) reduce to

$$\frac{\partial B_z}{\partial t} = \left(x\frac{\partial}{\partial y} + y\frac{\partial}{\partial x}\right)v_z, \tag{4}$$

$$\frac{\partial v_z}{\partial t} = \left(x\frac{\partial}{\partial y} + y\frac{\partial}{\partial x}\right)B_z. \tag{5}$$

The x and y components of the induction and momentum equations have the trivial solution $B_x = B_y = v_x = v_y = 0$. In this case, with the assumption of invariance in the z-direction, it follows from the continuity equation that the perturbations described by (4) and (5) are incompressible, i.e. they are shear Alfvén waves. It is evident from these equations that B_z satisfies

$$\frac{\partial^2 B_z}{\partial t^2} = \left(x\frac{\partial}{\partial y} + y\frac{\partial}{\partial x}\right)^2 B_z. \tag{6}$$

This can be reduced to the one-dimensional wave equation

$$\frac{\partial^2 B_z}{\partial t^2} = \frac{\partial^2 B_z}{\partial u^2}, \tag{7}$$

using the coordinate transformation

$$x = \varphi^{1/2}\cosh u, \qquad y = \varphi^{1/2}\sinh u. \tag{8}$$

We consider the following solution of (7):

$$B_z = \sum_{n=1}^{25} \exp(-0.01n^2)\exp\left[-\left(\frac{\varphi - 0.2}{\Delta\varphi}\right)^2\right]\sin[k(u-u_-)]\cos kt, \tag{9}$$

where $\Delta\varphi$ is a constant,

$$k = \frac{n\pi}{u_+ - u_-} \tag{10}$$

and

$$u_\pm = \frac{1}{2}\ln\left|\frac{1}{\varphi} \pm \sqrt{\frac{1}{\varphi^2} - 1}\right|. \tag{11}$$

This solution has the property that $B_z = 0$ on the boundary $r = (x^2 + y^2)^{1/2} = 1$. Such a condition implies zero Poynting flux through the boundary, and thus conservation of total wave energy (field energy plus kinetic energy) within the domain $r \leqslant 1$.

Putting $\mathbf{B}_\mathrm{E} = \nabla \times (\psi_\mathrm{E}\hat{\mathbf{z}})$, it is evident from (1) that (in dimensionless units)

$$\psi_\mathrm{E} = \tfrac{1}{2}(y^2 - x^2). \tag{12}$$

From (8), it is then apparent that $\varphi = -2\psi_\mathrm{E}$, i.e. φ is constant on a flux surface of the unperturbed field; the variable u is a function of distance in the (x, y) plane along an unperturbed flux surface. The particular solution represented by (9) was chosen in order to distinguish clearly the behaviour of the shear wave from that of the fast wave in the X-point configuration. The φ-dependant exponential factor, with $\Delta\varphi$ set equal to a value much less than unity, ensures that the initial disturbance is strongly confined in φ space to the neighbourhood of one particular unperturbed

https://doi.org/10.1017/S0022377805004277 Published online by Cambridge University Press

flux surface. Since the solution represents a shear wave, there is no propagation of the pulse across the unperturbed field, and so the solution remains strongly localized in φ space for all time. By making the exponential factor peak at $\varphi = 0.2$, we ensure that the solution never approaches the vicinity of the X-point null at $r = 0$. In contrast, fast wave solutions of (2) and (3) can propagate to the null. Due to the spatial dependence of the local Alfvén speed, this leads to profile steepening and consequently resistive dissipation of wave energy (Craig and Watson 1992).

Figure 1 shows the shear wave solution given by (9) at three times, for $\Delta\varphi = 0.05$. There is some broadening of the pulse along the unperturbed magnetic field, but it remains confined to one quadrant of the X-point and, as noted previously, there is no propagation across the unperturbed field.

With B_z given by (9), it follows immediately from (5) that

$$v_z = \sum_{n=1}^{25} \exp(-0.01n^2) \exp\left[-\left(\frac{\varphi - 0.2}{\Delta\varphi}\right)^2\right] \cos[k(u - u_-)] \sin kt. \tag{13}$$

In our dimensionless units, the total shear wave energy per unit length in the z-direction is given by

$$\varepsilon_s = \iint (\tfrac{1}{2}B_z^2 + \tfrac{1}{2}v_z^2)\, dx\, dy, \tag{14}$$

where the domain of integration is the interior of the circle $r = 1$. It can be shown from (9) and (13) that ε is a conserved quantity, in accordance with the use of an ideal MHD model and the vanishing of Poynting flux at the system boundary. The temporal variation of the field (ε_{sf}) and kinetic (ε_{sk}) energy components, plotted in Fig. 2 for two different values of $\Delta\varphi$, is somewhat reminiscent of that found for the fast wave in the ideal limit by McClements et al. (2004): in both cases the energy components approach equipartition after a transient oscillatory phase, with oscillations occurring on the Alfvén timescale. Comparing the upper and lower frames of Fig. 2, we observe that the time taken to reach equipartition is reduced if the width of the initial field perturbation is increased. The damping of oscillations apparent in Fig. 2 is a consequence of phase mixing, noted previously by Hassam and Lambert (1996) to be a characteristic feature of shear waves in X-point field configurations.

3. Wave coupling at X-point with longitudinal field

3.1. Ideal limit

We now introduce a small steady longitudinal component to the equilibrium field configuration, $B_{z0} = B_0/\lambda$ where $\lambda \gg 1$. In dimensionless units, the full equilibrium field is then

$$\mathbf{B}_E = y\hat{\mathbf{x}} + x\hat{\mathbf{y}} + \frac{1}{\lambda}\hat{\mathbf{z}}. \tag{15}$$

Putting

$$\mathbf{B} = \mathbf{B}^{(0)} + \frac{1}{\lambda}\mathbf{B}^{(1)} + \cdots, \tag{16}$$

$$\mathbf{v} = \mathbf{v}^{(0)} + \frac{1}{\lambda}\mathbf{v}^{(1)} + \cdots, \tag{17}$$

https://doi.org/10.1017/S0022377805004277 Published online by Cambridge University Press

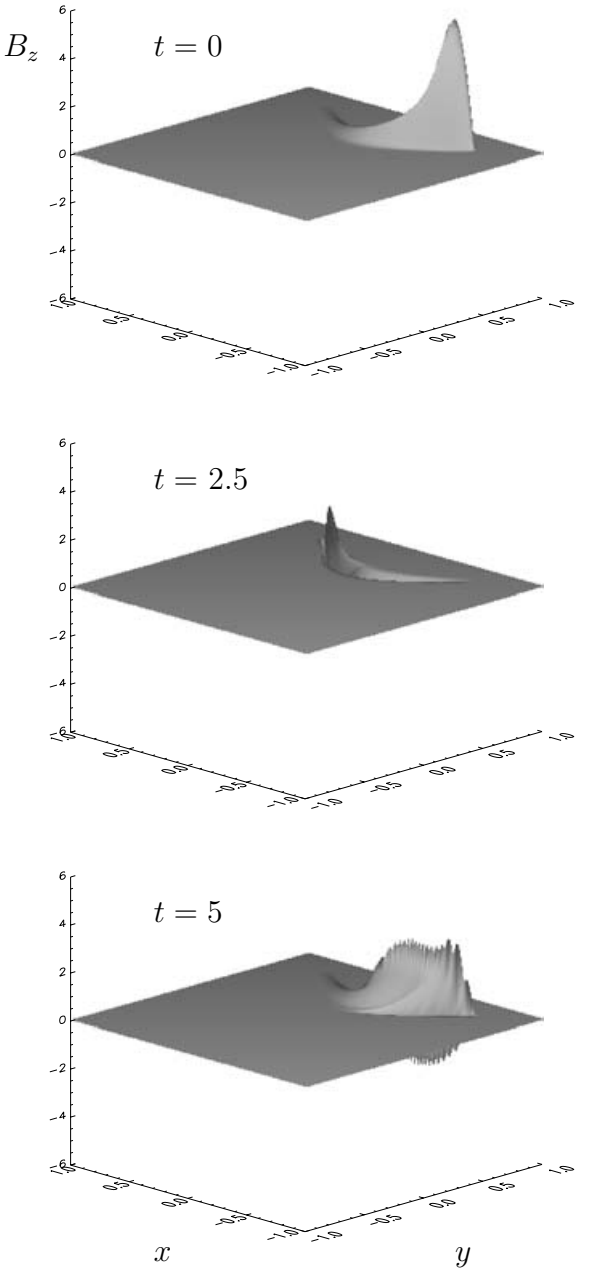

Figure 1. Shear wave B_z solution for $\Delta\varphi = 0.05$ at $t = 0$ (top), 2.5 (middle) and 5 (bottom) Alfvén times. The units of B_z are arbitrary; x and y are normalized to the system size r_0.

the ideal MHD induction and momentum equations become

$$\left[\frac{\partial \mathbf{B}^{(0)}}{\partial t} + \frac{1}{\lambda}\frac{\partial \mathbf{B}^{(1)}}{\partial t} + \cdots\right] = \nabla \times \left[\left(\mathbf{v}^{(0)} + \frac{1}{\lambda}\mathbf{v}^{(1)} + \cdots\right) \times \left(y\hat{\mathbf{x}} + x\hat{\mathbf{y}} + \frac{1}{\lambda}\hat{\mathbf{z}}\right)\right], \quad (18)$$

https://doi.org/10.1017/S0022377805004277 Published online by Cambridge University Press

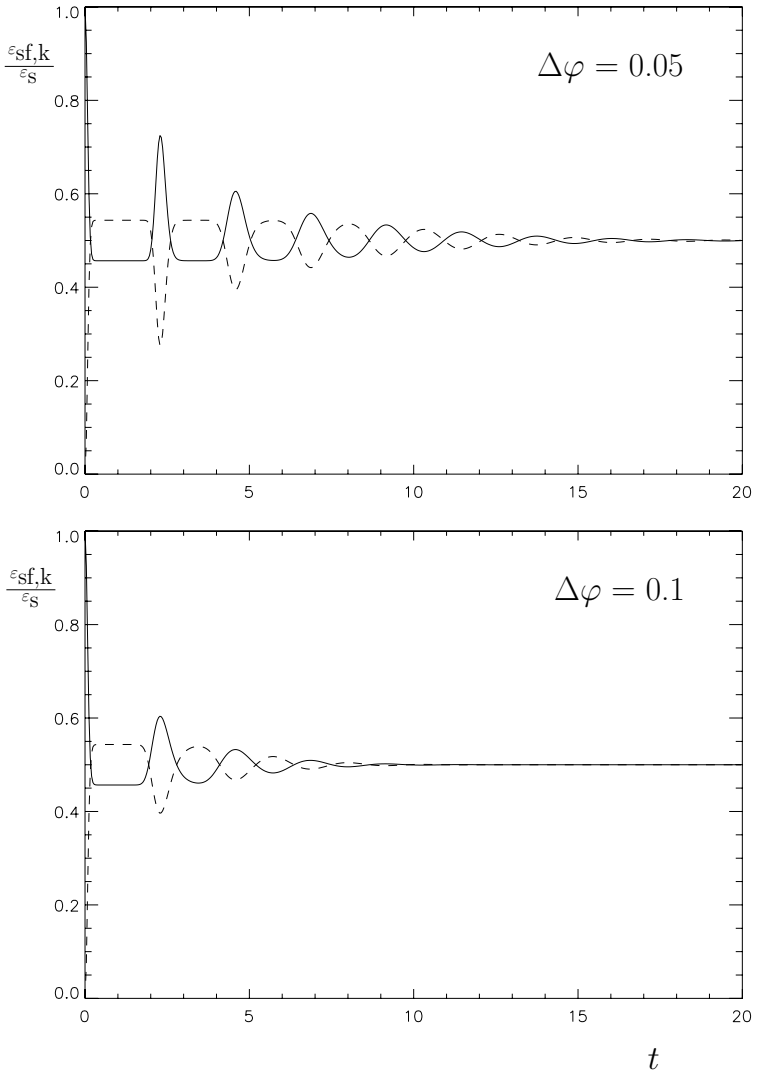

Figure 2. Normalized field energy ε_{sf} (solid) and kinetic energy ε_{sk} (dashed) versus time for the shear wave solution, with $\Delta\varphi$ equal to 0.05 (top) and 0.1 (bottom).

$$\left[\frac{\partial \mathbf{v}^{(0)}}{\partial t} + \frac{1}{\lambda}\frac{\partial \mathbf{v}^{(1)}}{\partial t} + \cdots\right] = \left[\nabla \times \left(\mathbf{B}^{(0)} + \frac{1}{\lambda}\mathbf{B}^{(1)} + \cdots\right)\right] \times \left(y\hat{\mathbf{x}} + x\hat{\mathbf{y}} + \frac{1}{\lambda}\hat{\mathbf{z}}\right). \quad (19)$$

Equating terms independent of λ, and taking the z-components, we obtain (4) and (5). Thus, to leading order the solution obtained previously for the shear wave, (9) and (13), can still be used. We consider the case in which these equations give the complete zeroth-order solution, i.e. we take $B_x^{(0)} = B_y^{(0)} = v_x^{(0)} = v_y^{(0)} = 0$. Equating terms proportional to $1/\lambda$ in (18) and (19), we then obtain

$$\frac{\partial \mathbf{B}^{(1)}}{\partial t} = \nabla \times [\mathbf{v}^{(1)} \times (y\hat{\mathbf{x}} + x\hat{\mathbf{y}})], \quad (20)$$

https://doi.org/10.1017/S0022377805004277 Published online by Cambridge University Press

$$\frac{\partial \mathbf{v}^{(1)}}{\partial t} - (\nabla \times \mathbf{B}^{(1)}) \times (y\hat{\mathbf{x}} + x\hat{\mathbf{y}}) = -\frac{\partial B_z^{(0)}}{\partial x}\hat{\mathbf{x}} - \frac{\partial B_z^{(0)}}{\partial y}\hat{\mathbf{y}}. \tag{21}$$

We first note that the z components of (20) and (21) are identical to the homogeneous pair of equations (4) and (5), with trivial solution $B_z^{(1)} = v_z^{(1)} = 0$. Writing

$$\mathbf{B}^{(1)} = \nabla \times (\psi \hat{\mathbf{z}}) \tag{22}$$

and

$$w = x v_x^{(1)} - y v_y^{(1)}, \tag{23}$$

we find that the x and y components of the momentum equation (21) can be combined to give

$$\frac{\partial w}{\partial t} - r^2 \nabla^2 \psi = -x \frac{\partial B_z^{(0)}}{\partial x} + y \frac{\partial B_z^{(0)}}{\partial y}, \tag{24}$$

and that the induction equation (20) reduces to

$$\frac{\partial \psi}{\partial t} = w. \tag{25}$$

Equations (24) and (25) describe the temporal evolution of a fast wave driven perturbatively by a shear wave in the presence of a small longitudinal magnetic field. Craig and McClymont (1991) noted that in the framework of resistive MHD only azimuthally symmetric fast wave perturbations to a two-dimensional X-point are associated with topological reconnection, i.e. dissipation of field energy. Partly with this observation in mind, we now focus our attention on the azimuthally symmetric component of the fast wave field. Writing

$$\psi = \sum_{m=-\infty}^{\infty} \psi_m e^{im\theta}, \tag{26}$$

$$w = \sum_{m=-\infty}^{\infty} w_m e^{im\theta}, \tag{27}$$

where θ is the azimuthal angle in the (x, y) plane, we infer from (24) and (25) that the azimuthally symmetric components of w and ψ satisfy the equations

$$\frac{\partial w_0}{\partial t} - r \frac{\partial}{\partial r}\left(r \frac{\partial \psi_0}{\partial r} \right) = \int_0^{2\pi} \left[-x \frac{\partial B_z^{(0)}}{\partial x} + y \frac{\partial B_z^{(0)}}{\partial y} \right] \frac{d\theta}{2\pi}, \tag{28}$$

$$\frac{\partial \psi_0}{\partial t} = w_0. \tag{29}$$

Except for the presence of the shear wave drive term, (28) and (29) represent the ideal MHD limit of a pair of equations studied by two of the present authors in an earlier paper (McClements et al. 2004): we have adapted the finite difference numerical scheme used in that paper for the purpose of solving (28) and (29). As stated previously, we take $\mathbf{B}_z^{(0)}$ to be given by (9); the integral on the right-hand side of (28) must then be computed for each time step numerically. We adopt the same boundary conditions for the fast wave as those invoked in our earlier paper, namely $\partial \psi_0 / \partial r = 0$ at both $r = 0$ and $r = 1$. The fast wave field must equal zero at the inner boundary to ensure regularity and consistency with the linear approximation (McClements et al. 2004): as in the case of the shear wave, by forcing the magnetic field to be zero on the outer boundary we ensure that there

https://doi.org/10.1017/S0022377805004277 Published online by Cambridge University Press

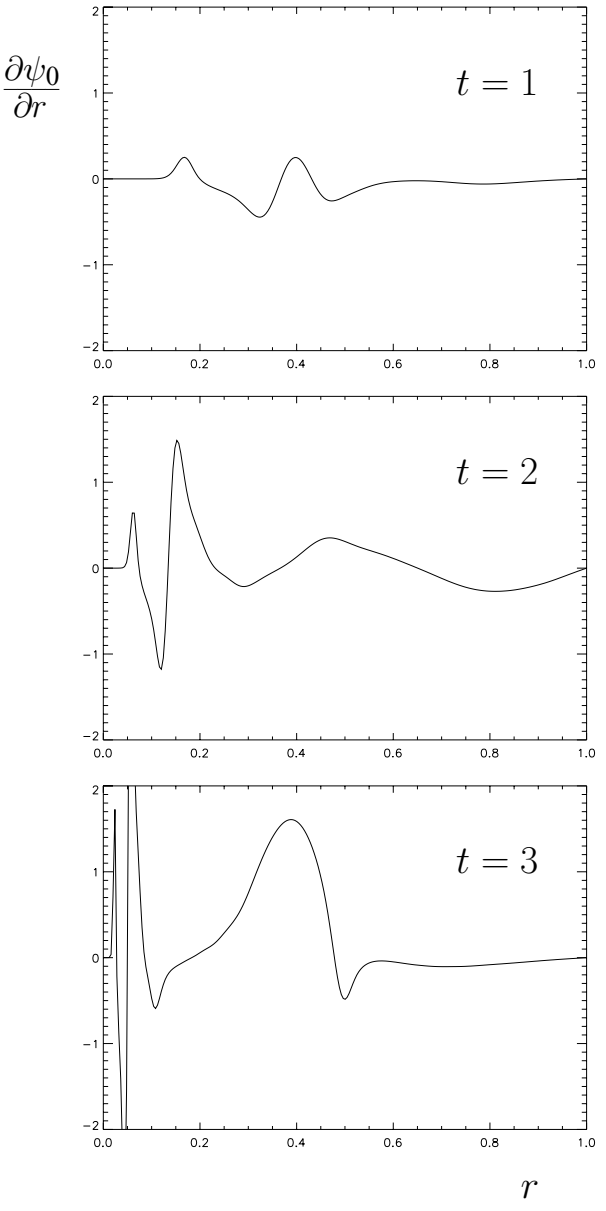

Figure 3. Radial profile of the azimuthally symmetric component of the fast wave magnetic field $\partial\psi_0/\partial r$ at $t = 1$ (top), $t = 2$ (middle) and $t = 3$ (bottom) Alfvén times in the ideal limit. The radius r is normalized to the system size r_0 and the units of the fast wave field are arbitrary.

is zero Poynting flux out of the system. For all of the scenarios considered in the remainder of this paper, computations were performed using various space and time steps to ensure convergence of numerical results.

We consider the case of an initial state in which only a shear wave is present, with field and velocity profiles given by (9) and (13), $\Delta\varphi$ being set equal to 0.05. For this scenario, Fig. 3 shows the $m = 0$ component of the fast wave field $\partial\psi_0/\partial r$

https://doi.org/10.1017/S0022377805004277 Published online by Cambridge University Press

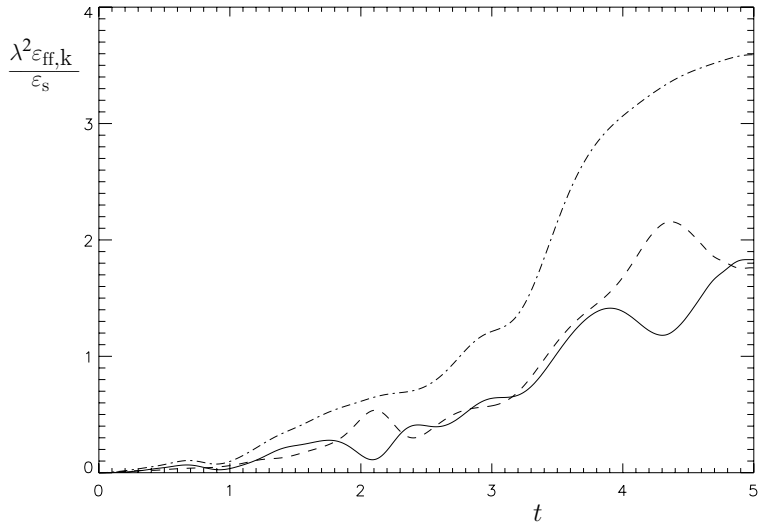

Figure 4. Time variation in the ideal limit of the azimuthally symmetric components of the fast wave magnetic field energy (solid curve), kinetic energy (dashed curve) and total energy (dashed-dotted curve). The energy components are normalized to $\varepsilon_{\mathrm{s}}/\lambda^2$, where ε_{s} is the total energy in the shear wave.

at three different times. It is apparent that energy is being channelled via the fast wave into the null at $r = 0$ on an Alfvénic timescale. It is also striking that sharp gradients rapidly appear in the field profile: this is due to the spatial dependence of the local Alfvén speed, noted previously. The rapidity of this profile steepening suggests that resistive and non-ideal effects are likely to become important after only a few Alfvén times at most.

The azimuthally symmetric components of the fast wave field energy $\varepsilon_{\mathrm{ff}}$ and kinetic energy $\varepsilon_{\mathrm{fk}}$ per unit length in the z-direction are given by

$$\varepsilon_{\mathrm{ff}} = \frac{1}{2\lambda^2}\iint\left(\frac{\partial\psi_0}{\partial r}\right)^2 dx\,dy. \tag{30}$$

$$\varepsilon_{\mathrm{fk}} = \frac{1}{2\lambda^2}\iint\left(\frac{w_0}{r}\right)^2 dx\,dy. \tag{31}$$

Figure 4 shows $\varepsilon_{\mathrm{ff}}$ (solid curve), $\varepsilon_{\mathrm{fk}}$ (dashed curve) and the sum of these (dashed-dotted curve) as functions of time in the ideal limit. The energy components are normalized to $\varepsilon_{\mathrm{s}}/\lambda^2$, where ε_{s} is the total energy in the shear wave (in our perturbative approach, the latter quantity is assumed to be constant). The fast wave energy rises rapidly over time, as one would expect, but the rate of increase is not constant. Moreover, there are local minima in the field energy plot, coinciding with local maxima in the kinetic energy, and occurring at intervals of about one Alfvén time. These maxima and minima appear to reflect the oscillations between field and kinetic energy that occur in the shear wave solution prior to equipartition (Fig. 2). The normalized fast wave energy approaches unity after only about three Alfvén times. Although the use of a perturbative approach does not allow us to choose λ to be of order unity, the results in Fig. 4 suggest nevertheless that a significant

https://doi.org/10.1017/S0022377805004277 Published online by Cambridge University Press

fraction of the shear wave energy would be converted to fast wave energy on an Alfvénic timescale at an X-point with $B_{z0} \sim B_0$.

3.2. Resistive effects

We now consider the effects of adding a resistive diffusion term to (29):

$$\frac{\partial \psi_0}{\partial t} = w_0 + \frac{1}{Sr}\frac{\partial}{\partial r}\left(r\frac{\partial \psi_0}{\partial r}\right), \tag{32}$$

where $S \equiv \mu_0 r_0 c_{\rm A0}/\eta$, $c_{\rm A0}$ being the Alfvén speed corresponding to the field B_0 and η the resistivity (McClements et al. 2004). It is important to note that the Lundquist number S is proportional to an equilibrium magnetic field that vanishes as $r_0 \rightarrow 0$, and therefore S itself need not be a very large number in order to be realistic. Strictly speaking, the use of resistive MHD to model the fast wave and ideal MHD to model the shear wave is inconsistent, since both types of wave can undergo profile steepening and hence dissipation in a non-uniform plasma. However, because the shear wave does not propagate into the X-point null, it is not subject to the very rapid (Alfvén timescale) steepening associated with the fast wave.

We have solved numerically (28) and (32) for $S = 10^2$–10^6, using the shear wave drive term invoked in the ideal case (with $\Delta\varphi$ again being set equal to 0.05), and from these solutions we have computed the temporal evolution of the azimuthally symmetric fast wave energy components: the results are shown in Fig. 5. As in the ideal limit, the variation of fast wave energy components with time is non-monotonic, reflecting the transient variations of field and kinetic energy in the shear wave driver. At any given time the energy in the azimuthally symmetric component of the fast wave is progressively reduced as the resistivity is increased, with the field energy and kinetic energy decaying at essentially the same rate, as in the non-driven scenario considered in our previous paper (McClements et al. 2004). Figure 5 indicates that most of the energy channelled into the azimuthally symmetric component of the fast wave in the ideal limit is dissipated after a few Alfvén times when the resistivity is high. The shear Alfvén wave is thus effectively heating the plasma, due to the presence of a steady longitudinal magnetic field component.

3.3. Electron inertial effects

McClements et al. (2004) showed that the temporal behaviour of a fast wave in X-point geometry can be strongly modified by the presence of the electron inertial ($\partial \mathbf{j}/\partial t$) term in Ohm's law:

$$\mathbf{E} + \mathbf{v} \times \mathbf{B} = \eta \mathbf{j} + \frac{m_{\rm e}}{ne^2}\frac{\partial \mathbf{j}}{\partial t}. \tag{33}$$

Here, n is particle density, $m_{\rm e}$ is electron mass and e is the electron charge. Neglecting other non-MHD terms in the generalised Ohm's law, the induction equation then becomes

$$\frac{\partial}{\partial t}\left[\psi_0 - \frac{\delta_{\rm e}^2}{r}\frac{\partial}{\partial r}\left(r\frac{\partial \psi_0}{\partial r}\right)\right] = w_0 + \frac{1}{Sr}\frac{\partial}{\partial r}\left(r\frac{\partial \psi_0}{\partial r}\right), \tag{34}$$

where $\delta_{\rm e} = c/(\omega_{\rm pe} r_0)$ is the collisionless skin depth normalized to the system size, c being the speed of light and $\omega_{\rm pe}$ the electron plasma frequency. We have solved (28) and (34) for the same initial conditions as before and $S = 10^4$, with $\delta_{\rm e}$

https://doi.org/10.1017/S0022377805004277 Published online by Cambridge University Press

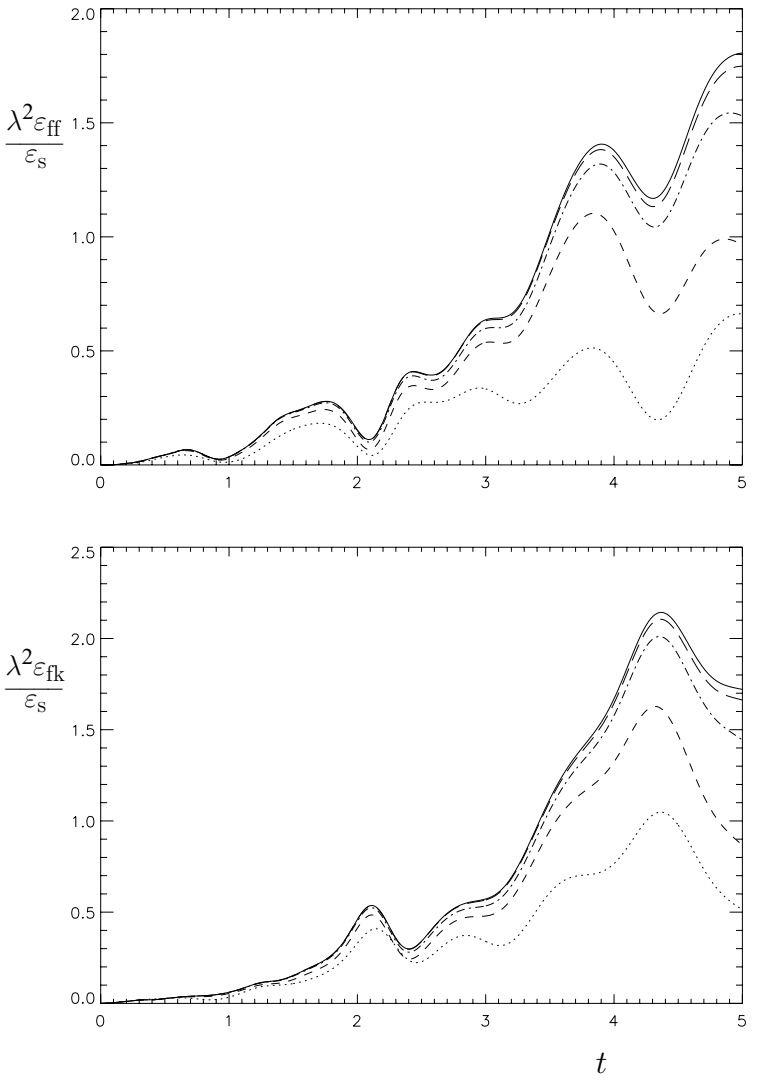

Figure 5. Temporal evolution of the azimuthally symmetric component of the fast wave field energy (top) and kinetic energy (bottom) for $S = 10^6$ (solid curves), 10^5 (long dashed curves), 10^4 (dotted-dashed curves), 10^3 (short dashed curves) and 10^2 (dotted curves). Electron inertial effects are neglected.

ranging from 10^{-3} to 10^{-1}. The temporal evolution of the azimuthally symmetric energy components are shown in Fig. 6. In this case the kinetic energy includes a contribution $\varepsilon_{\rm fke}$ from the electrons given by (McClements et al. 2004)

$$\varepsilon_{\rm fke} = \frac{1}{2\lambda^2}\iint \delta_{\rm e}^2(\nabla^2\psi_0)^2 dx\,dy. \tag{35}$$

The results for $\delta_{\rm e} = 10^{-3}$ are essentially identical to those obtained previously in the MHD limit (the dotted-dashed curves in Fig. 5), and a factor of ten increase in $\delta_{\rm e}$ to 10^{-2} has very little effect. In both of these cases the electrons make only a small contribution to the wave kinetic energy.

https://doi.org/10.1017/S0022377805004277 Published online by Cambridge University Press

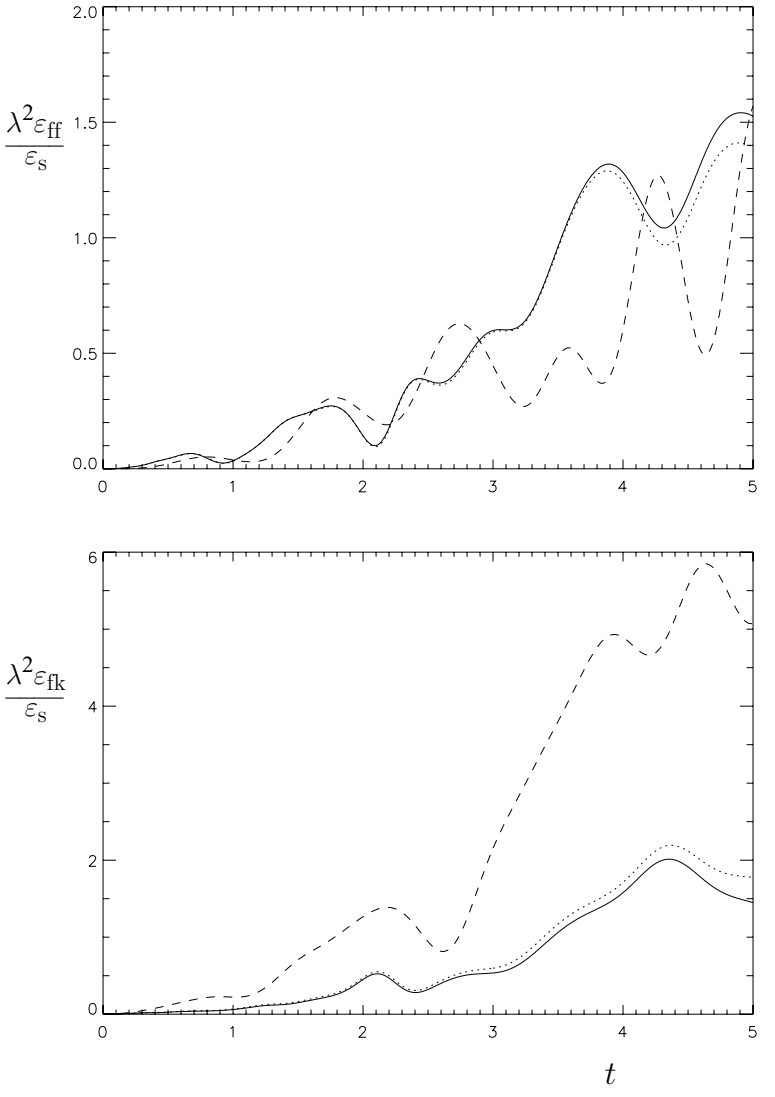

Figure 6. Temporal evolution of the azimuthally symmetric component of the fast wave field energy (top) and kinetic energy (bottom) for $\delta_{\rm e} = 10^{-3}$ (solid curves), $\delta_{\rm e} = 10^{-2}$ (dotted curves) and $\delta_{\rm e} = 10^{-1}$ (dashed curves). The Lundquist number is $S = 10^4$.

The temporal behaviour of the energy components changes dramatically when the skin depth is increased to 10^{-1}: after about three Alfvén times the energy is predominantly kinetic, and the field energy fluctuations are not in phase with those observed at lower $\delta_{\rm e}$. The electron kinetic energy is then comparable to the ion kinetic energy. In absolute terms, the fraction of shear wave energy channelled into electron and ion flows after a few Alfvén times is several times higher than that found in the MHD case, whereas the energy in the fast wave field in this period is comparable to or less than the MHD value. Indeed, for $S = 10^4$, $\delta_{\rm e} = 0.1$ the fast wave kinetic energy at $t = 5$ is even greater than the total (kinetic plus field) fast wave energy found at this time in the ideal limit (Fig. 4). Another distinguishing feature of the $\delta_{\rm e} = 0.1$, $S = 10^4$ case is that the steepest profile gradients, and the

https://doi.org/10.1017/S0022377805004277 Published online by Cambridge University Press

greatest contributions to the field and kinetic energy components, occur far from the X-point null at $r = 0$. In the calculations with lower δ_e, the profiles are similar to those found in the ideal limit, with the strongest gradients occurring close to $r = 0$ (Fig. 3).

This behaviour can be understood in terms of results obtained by McClements and Thyagaraja (2004) and McClements et al. (2004). The dimensionless parameter $2S\delta_e^2$ can be identified as the collision time normalized to the Alfvén time, or equivalently as the square of the ratio of the collisionless skin depth to the resistive length scale. In the collision-dominated (MHD) regime, when $S\delta_e^2 < 1$, it can be shown that a two-dimensional ($B_{z0} = 0$) current-free X-point is characterized by a discrete spectrum of fast wave eigenmodes (Craig and McClymont 1991; McClements and Thyagaraja 2004). In the weakly collisional regime defined by $S\delta_e^2 \gg 1$ this discrete spectrum ceases to exist: instead there is a continuum of modes with an intrinsic damping rate equal to the normalized collision frequency, $1/2S\delta_e^2$, which determines the overall dissipation rate. However, since the field energy of an undriven fast wave decays on a much shorter (Alfvén) timescale, due to continuum damping, the energy after a few Alfvén times is almost entirely kinetic in this regime. Thus, when the collisionless skin depth (δ_e) exceeds the resistive length scale ($S^{-1/2}$), the energy in a shear wave approaching an X-point with finite B_{z0} is rapidly transformed into plasma kinetic energy: in a warm plasma fluid model, one would expect heating to occur in addition to fluid acceleration. The differences in the evolution of field and velocity profiles in the regimes of strong and weak collisionality can be attributed to the fact that for $S\delta_e^2 > 1$ every point in the solution domain is associated with a singular eigenmode, whereas in the MHD limit only the point $r = 0$ is singular (McClements and Thyagaraja 2004).

4. Summary and discussion

We have investigated the coupling of shear and fast Alfvén waves in the vicinity of a magnetic X-point with a weak longitudinal guide field, neglecting variations in the longitudinal direction and plasma pressure effects. Specifically, we have computed the rate at which the energy of a shear Alfvén wave is channelled into the azimuthally symmetric component of a fast wave, and the rates at which the field energy and kinetic energy of the latter wave are dissipated or converted into other forms of energy when resistive and electron inertial effects are taken into account. We have shown that shear wave energy is most rapidly and efficiently converted to plasma kinetic energy when the collisionless skin depth exceeds the resistive scale length, i.e. in the weakly collisional regime.

The perturbative analysis of Sec. 3 is valid for $r > 1/\lambda$ (Bulanov et al. 1992). As noted previously, in the weakly collisional regime ($S\delta_e^2 > 1$) the strongest field and velocity gradients, and the greatest contributions to the field and kinetic energy, occur far from $r = 0$. Results obtained in this limit are likely to be more robust, in terms of their applicability to configurations with specific finite values of λ, than those of the MHD regime, in which the strongest gradients are found close to the null, i.e. in the region of the solution domain where the perturbation analysis is most likely to break down. McClements et al. (2004) noted that the restriction on the validity of the linear approximation also becomes less severe as $S\delta_e^2$ is increased, for similar reasons.

We now discuss possible applications of this work. Mode coupling at X-points with finite B_{z0} could be significant for solar coronal heating since, although shear Alfvén

waves have been detected directly in the solar wind (Balogh et al. 1995), and provide an effective means of transporting energy from the photosphere to the upper layers of the solar atmosphere, the mechanism whereby this energy could most effectively be deposited in the coronal plasma remains unclear. In one widely studied scenario, shear Alfvén wave dissipation arises from phase mixing associated with profile steepening in the presence of a density gradient perpendicular to the magnetic field (e.g. Botha et al. 2000). Alternatively, dissipation could be a secondary process, resulting from mode conversion. Magnetic X-points with $B_{z0} \neq 0$, which are likely to be present in the corona, provide a mechanism for the conversion of shear waves into fast waves, and the subsequent dissipation or conversion of fast wave energy via steepening of the wave profile (McClements et al. 2004). It is unclear which of the collisionality regimes defined in Sec. 3 is more likely to apply to the corona. Since magnetic fields cannot be measured directly in the corona, it is also uncertain what values of λ might be appropriate for this environment. In any case, our results suggest that a significant fraction of the energy of a shear Alfvén wave encountering an X-point with finite B_{z0} would be converted to heat or flow energy on an Alfvén timescale. A similar process, on a larger scale, could in principle lead to the explosive release of magnetic field energy known as a solar flare: McClements et al. (2004) showed that damping of non-potential magnetic field energy at a two-dimensional X-point provides a possible framework for understanding the most rapid (sub-second) fluctuations yet observed in flare hard X-ray emission.

Any comments on the possible relevance of this work for tokamaks are necessarily tentative, since in these devices the magnetic field is predominantly toroidal, i.e. $B_{z0} > B_0$: the opposite ordering was assumed in the above analysis. Moreover, we have neglected a wide range of effects (finite plasma pressure, toroidal field line bending, equilibrium currents and flows, finite Larmor radius and variations in the longitudinal direction) that are known to be important under tokamak conditions. One can make a number of qualitative remarks, nevertheless. For any finite longitudinal field there is linear mode conversion from the incompressible shear wave to the compressible fast wave (Bulanov et al. 1992). We suggest that a mode conversion process of this type could play a role in the triggering of edge-localized modes (ELMs), short periodic bursts of particle and heat flux that commonly occur during H-mode in divertor tokamaks. Myra et al. (1997) found that the X-points of divertor tokamak plasmas have a significant effect on the stability of ballooning modes, which are believed to be associated with ELMs. The tendency of an X-point to convert shear waves to fast waves, and the dissipation of the latter due to resistive or non-MHD effects, suggest a mechanism whereby the energy in ballooning modes could be converted to the particle and heat fluxes associated with ELMs.

Acknowledgements

This work was funded jointly by the United Kingdom Engineering and Physical Sciences Research Council and by EURATOM.

References

Balogh, A., Smith, E. J., Tsuritani, B. T., Southwood, D. J., Forsyth, R. J. and Horbury, T. S. 1995 *Science* **268**, 1007.

Botha, G. J. J., Arber, T. D., Nakariakov, V. M. and Keenan, F. P. 2000 *Astron. Astrophys.* **363**, 1186.

Browning, P. K. and Vekstein, G. E. 2001 *J. Geophys. Res.* **106**, 18 677.

Bruhwiler, D. L. and Zweibel, E. G. 1992 *J. Geophys. Res.* **97**, 10 825.

Bulanov, S. V. 1980 *Sov. Astron. Lett.* **6**, 206.

Bulanov, S. V. and Syrovatskii, S. I. 1980 *Sov. J. Plasma Phys.* **6**, 661.

Bulanov, S. V., Shasharina, S. G. and Pegoraro, F. 1992 *Plasma Phys. Control. Fusion* **34**, 33.

Craig, I. J. D. and McClymont, A. N. 1991 *Astrophys. J.* **371**, L41.

Craig, I. J. D. and Watson, P. G. 1992 *Astrophys. J.* **393**, 385.

Donné, A. J. H., van Gorkom, J. C., Udintsev, V. S., Domier, C. W., Krämer-Flecken, A., Luhmann Jr., N. C., Schüller, F. C. and TEXTOR team 2005 *Phys. Rev. Lett.* **94**, 08 5001.

Hamilton, B., McClements, K. G., Fletcher, L. and Thyagaraja, A. 2003 *Solar Phys.* **214**, 339.

Hamilton, B., Fletcher, L., McClements, K. G. and Thyagaraja, A. 2005 *Astrophys. J.* **625**, 496.

Hassam, A. B. and Lambert, R. P. 1996 *Astrophys. J.* **472**, 832.

McClements, K. G. and Thyagaraja, A. 2004 *Plasma Phys. Control. Fusion* **46**, 39.

McClements, K. G., Thyagaraja, A., Ben Ayed, N. and Fletcher, L. 2004 *Astrophys. J.* **609**, 423.

McLaughlin, J. A. and Hood, A. W. 2004 *Astron. Astrophys.* **420**, 1129.

Mori, K., Sakai, J. and Zhao, J. 1998 *Astrophys. J.* **494**, 430.

Myra, J. R., D'Ippolito, D. A. and Goedbloed, J. P. 1997 *Phys. Plasmas* **4**, 1330.

Petkaki, P. and MacKinnon, A. L. 1997 *Solar Phys.* **172**, 279.